ACS APPLIED MATERIALS & INTERFACES

Research Article

www.acsami.org

Capacitive and Oxidant Generating Properties of Black-Colored TiO_2 Nanotube Array Fabricated by Electrochemical Self-Doping

Choonsoo Kim, Seonghwan Kim, Jaehan Lee, Jiye Kim, and Jeyong Yoon*

School of Chemical and Biological Engineering, College of Engineering, Institute of Chemical Process, Seoul National University (SNU), Gwanak-gu, Daehak-dong, Seoul 151-742, Republic of Korea

Supporting Information

ABSTRACT: Recently, black-colored TiO_2 NTA (denoted as black TiO_2 NTA) fabricated by self-doping of TiO_2 NTA with the amorphous phase led to significant success as a visible-light-active photocatalyst. This enhanced photocatalytic activity is largely attributed to a higher charge carrier density as an effect of electrochemical self-doping resulting in a higher optical absorbance and lower transport resistance. Nevertheless, the potential of black TiO_2 NTA for other electrochemical applications, such as a supercapacitor and an oxidant-generating anode, has not been fully investigated. Here, we report the capacitive and oxidant generating properties of black TiO_2 NTA. The black TiO_2 NTA exhibited significantly a high value for areal capacitance with a good rate capability and novel electrocatalytic activity in generating $^{\bullet}OHs$ and Cl_2 compared to pristine TiO_2 NTA with the anatase phase. This study suggests that the black TiO_2 NTA be applied as a supercapacitor and an oxidant generating anode.

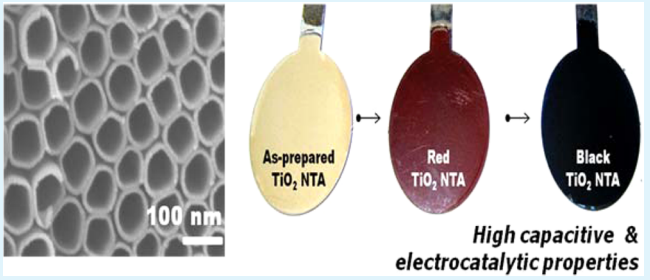

KEYWORDS: *TiO_2 nanotube array, electrochemical self-doping, electrochromism, capacitive and oxidant-generating properties*

1. INTRODUCTION

Since the discovery of anodized TiO_2 nanotube arrays (NTAs), TiO_2 NTA has been extensively studied as a novel material in various applications including dye-sensitized solar cells (DSSCs), photoelectrolysis cells, and sensors because of its photochemical properties, biocompatibility, low-cost, and simple preparation for fabricating nanostructures.[1−8] In addition, unique photocatalytic surface of TiO_2[9−11] has led to the exciting development of TiO_2 NTA as photocatalysts in energy conversion and water treatment.[12−15] TiO_2 NTA with these superior properties is often considered as the potential material for various electrochemical applications such as an electrode for capacitor and an oxidant generating system.[16−20]

However, electrochemical applications of TiO_2 NTA has been limited because of the poor electronic conductivity of TiO_2 resulting from its semiconductive nature.[21] To improve the electronic properties of TiO_2, there have been enormous efforts such as thermal hydrogenation, metallic and nonmetallic doping.[22] Despite the success with enhancing the electronic properties of TiO_2,[23,24] the complicated process of conventional doping methods was noted as the obstacle to further utilization.

On the other hand, electrochemical self-doping of TiO_2 NTA by cathodic polarization has emerged as one of the promising methods to enhance their electronic properties.[25,26] This change of electronic state in TiO_2 NTA accompanied by electrochromism is well explained by the proton intercalation ($Ti^{4+} + e^- + H^+ \rightarrow Ti^{3+}H^+$) possibly leading to the Ti^{3+} sites.[27,28] The blue-colored TiO_2 NTA (blue TiO_2 NTA) fabricated with the electrochemical self-doping of anatase TiO_2 NTA,[29−32] successfully demonstrated its possibility as the doping method.

Recently, black colored TiO_2 NTA (denoted as black TiO_2 NTA) was also fabricated with a novel strategy using electrochemical self-doping of amorphous TiO_2 NTA and annealing under nitrogen to provide high stability, and emerged as a visible-light-active photocatalyst.[33] According to our experiments (Supporting Information Figure S1), the black TiO_2 NTA can be only fabricated by the electrochemical self-doping of amorphous TiO_2 NTA, while the blue TiO_2 NTA is fabricated by the electrochemical self-doping of anatase TiO_2 NTA. Moreover, the black TiO_2 NTA exhibited the higher level of dopant than the blue TiO_2 NTA. It can be attributed to the larger spatial channel with the disordered structure and defects of amorphous TiO_2 NTA for the proton intercalation by the electrochemical self-doping than those of anatase TiO_2 NTA.[34,35] Nevertheless, the electrochemical properties and its application of black TiO_2 NTA have not been fully investigated. Therefore, the aim of this study was to examine the capacitive and oxidant generating properties of black TiO_2 NTA fabricated by electrochemical self-doping.

2. MATERIALS AND METHODS

Figure 1 shows a schematic diagram of the preparation for the black TiO_2 NTA fabricated with electrochemical self-doping and pristine TiO_2 NTA. As shown in Figure 1, the black TiO_2 NTA was prepared by

Received: August 1, 2014
Accepted: March 20, 2015
Published: March 20, 2015

DOI: 10.1021/acsami.5b00123
ACS Appl. Mater. Interfaces 2015, 7, 7486−7491

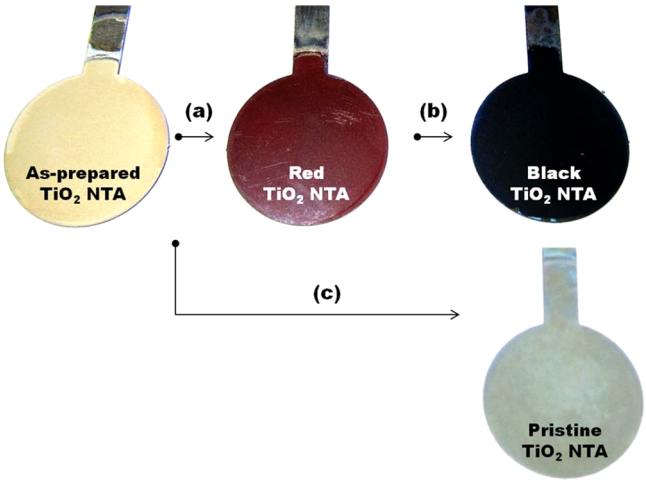

Figure 1. Schematic diagram showing the fabrication of the black TiO_2 NTA. The red TiO_2 NTA was prepared by thermal treatment at 200 °C under atmospheric conditions (a) and the black TiO_2 NTA was fabricated with electrochemical self-doping of the red TiO_2 NTA

electrochemical self-doping proposed by Zheng and co-workers.[33] This method was partially modified to reduce the undesired fragility of the nanotube layer on the fabricated black TiO_2 NTA with the addition of a thermal treatment step leading to the red colored TiO_2 NTA (denoted red TiO_2 NTA) before the electrochemical self-doping. In order to compare the electrochemical and surface properties of the black TiO_2 NTA, pristine TiO_2 NTA was prepared by the annealing of the as-prepared TiO_2 NTA at 450 °C for 1 h under atmospheric condition without electrochemical self-doping. The as-prepared and red TiO_2 NTA exhibited an amorphous phase, and the pristine TiO_2 NTA revealed an anatase phase (Figure S2 in Supporting Information). The fabricated black TiO_2 NTA is described in more detail below.

The as-prepared TiO_2 NTA with a working area of 2.54 cm^2 (d = 1.8 cm) was provided with anodization in an electrolyte containing H_2O (2.5 wt %)/NH_4F (0.2 wt %) with ethylene glycol for 5 h under a constant potential (45 V) at room temperature (25 °C). The as-prepared TiO_2 NTA was thermally treated at 200 °C for 1 h under atmospheric conditions leading to red TiO_2 NTA. The black TiO_2 NTA was fabricated with the electrochemical self-doping of red TiO_2 NTA with constant current (0.017 mA/cm^2) for 90 s in phosphate buffer solution ($[KH_2PO_4]_0$ = 0.1 M with NaOH, pH = 7.2) and annealing at 450 °C for 1 h under nitrogen (N_2) conditions.[33] The electrochemical self-doping exhibited a black coloration of the red TiO_2 NTA, which is well-known as the electrochromic effect resulting from the formation of Ti^{3+} sites, or oxygen vacancies by the cathodic polarization.[21,25]

The electro-generated $^{\bullet}OH$s were measured by UV−vis spectroscopy (Agilent 8453, Agilent Life Sciences and Chemical Analysis, USA) using *p*-nitrosodimethylaniline (RNO), which is well-known as a probe compound for $^{\bullet}OH$s.[36,37] The 20 μM of RNO was dissolved in phosphate buffer solution ($[KH_2PO_4]_0$ = 0.1 M with NaOH (pH = 7.2)). The RNO solution was electrolyzed under constant current (i = 0.05 A/cm^2), and the bleaching of RNO on the black TiO_2 and pristine TiO_2 NTA was monitored by UV−vis spectrometer at the adsorption of 440 nm.

The bleaching reaction rate of RNO can be explained by eq 1

$$-\frac{d[RNO]}{dt} = k[^{\bullet}OH]_{ss}[RNO] = k_{obs}[RNO] \quad (1)$$

From the integration of eq 1

$$-\ln\frac{[RNO]}{[RNO]_0} = k_{obs}t \quad (2)$$

where k is 1.25×10^{10} M^{-1} s^{-1},[38] [RNO] is the concentration of RNO ($[RNO]_0$ = 20 μM), $[^{\bullet}OH]_{ss}$ is the steady state concentration of $^{\bullet}OH$,

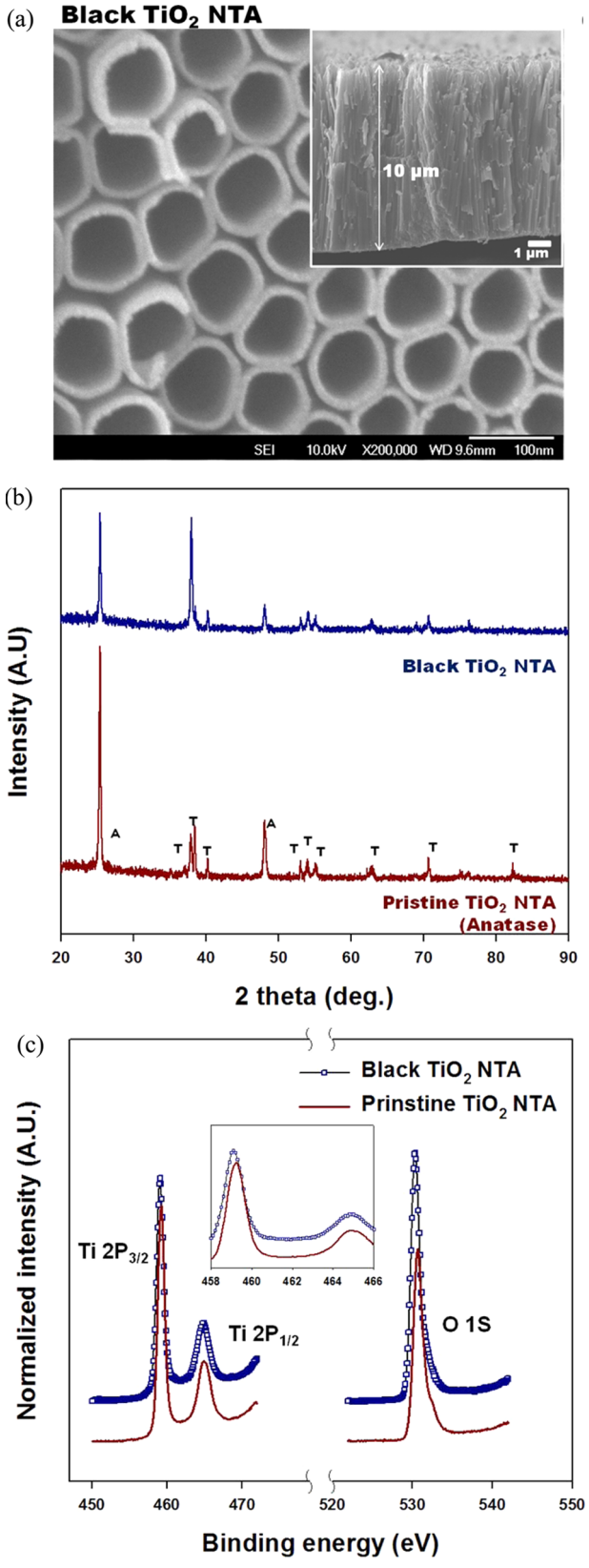

Figure 2. SEM image (a), XRD pattern (b), and XPS spectrum (c) of the black TiO_2 NTA and the pristine TiO_2 NTA. The inset of a shows the cross-sectional SEM image of the black TiO_2 NTA. The **A** and **T** in panel b mean anatase and titanium, respectively. The inset of c shows an enlarged XPS spectrum in the region of the Ti 2p peak.

DOI: 10.1021/acsami.5b00123
ACS Appl. Mater. Interfaces 2015, 7, 7486−7491

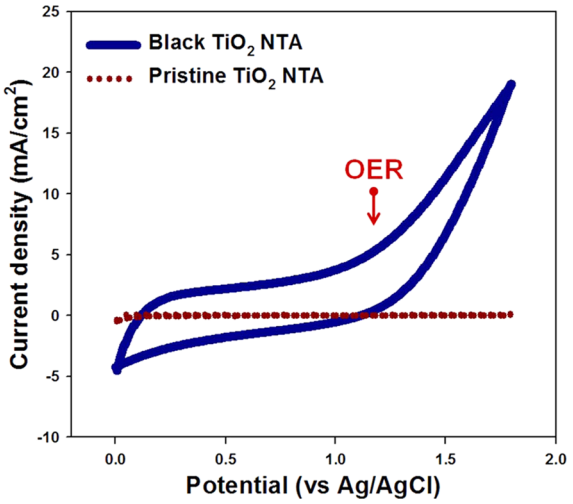

Figure 3. Cyclic voltammograms of the black TiO_2 NTA and pristine TiO_2 NTA obtained at a scan rate of 100 mV/s ($[KH_2PO_4]_0$ = 1 M with NaOH (pH = 7.2)).

and k_{obs} is the $k[^{\bullet}OH]_{ss}$ indicating the steady state production rate constant of $^{\bullet}OH$. This production rate was estimated by the slope of the semilog plot (eq 2), which was obtained from the assumption of pseudo-first-order kinetics. The produced amount of active chlorine was examined as milligrams per liter (as free Cl_2) with the *N*,*N*-diethyl-*p*-phenylenediamine (DPD) colorimetric method with a spectrophotometer (DR/2010, HACH Co., Loveland, USA) at 530 nm.[39]

Cyclic voltammetry and electrochemical impedance spectroscopy measurements were performed to analyze the electrochemical properties of the prepared black TiO_2 NTA and TiO_2 NTA. The measurements were conducted with a conventional three electrodes system using a computer-controlled potentiostat/galvanostat (PARSTAT 2273A, Princeton Applied Research, USA). The dopant level of black TiO_2 NTA was examined by the Mott–Schottky equation (eq 3)[40]

$$\frac{1}{C_{SC}^{\ 2}} = \left(\frac{2}{e\varepsilon_0\varepsilon N_D}\right)\left(-\Delta\Phi - \frac{kT}{e}\right) \quad (3)$$

where C_{SC} is the space charge capacitance ($\mu F^{-2}cm^4$), $-\Delta\Phi = E - E_{fb}$ (E is the applied potential and E_{fb} is the flat band potential), N_D is the donor density (cm^{-3}), e is the electronic charge, ε is the dielectric constant of electrode material, ε_0 is the permittivity of the free space, k is the Boltzmann constant, and T is the operating temperature. The values

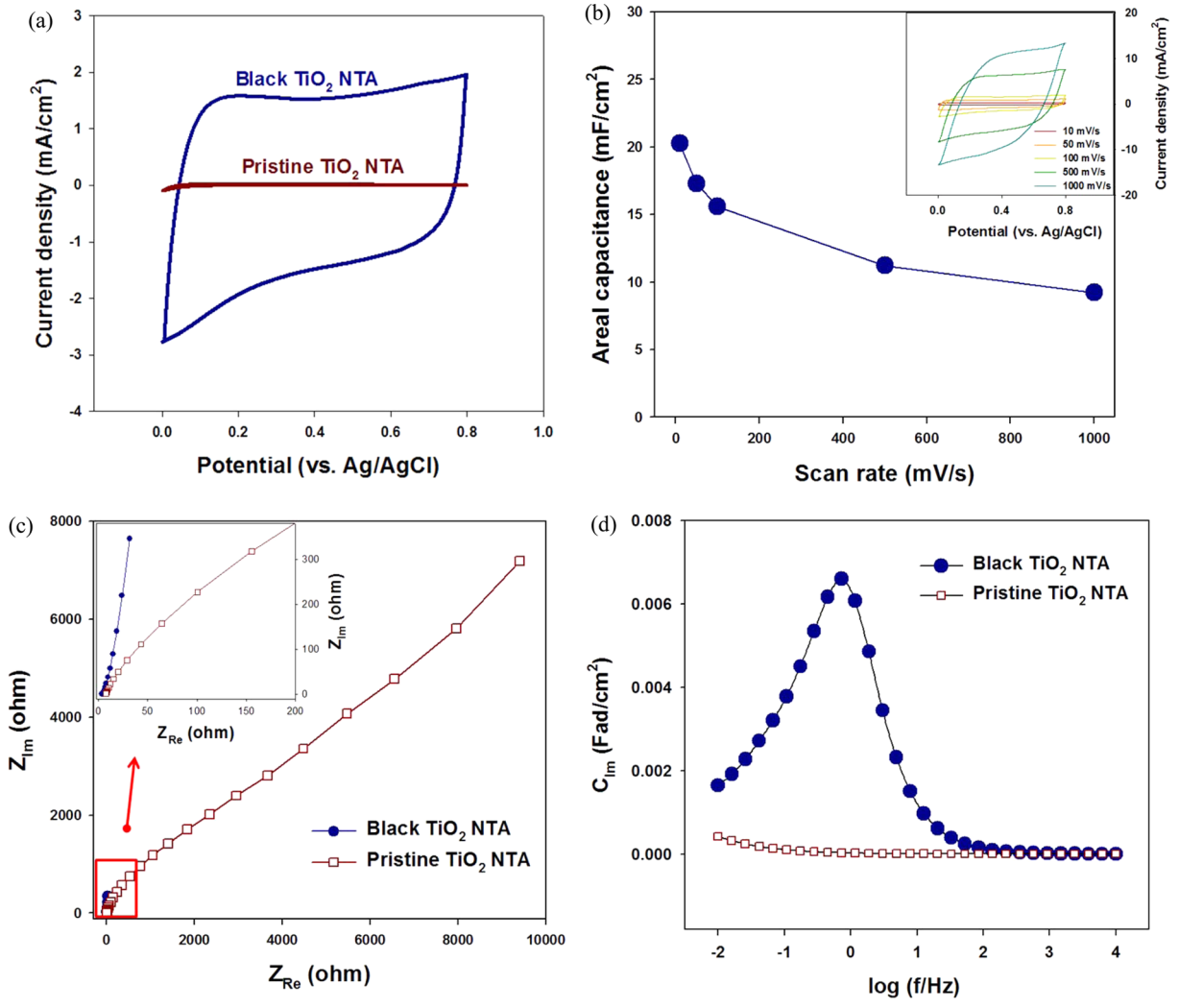

Figure 4. Comparison of cyclic voltammograms (a) for the black TiO_2 NTA and pristine TiO_2 NTA at a scan rate of 100 mV/s and (b) areal capacitance of the black TiO_2 NTA as a function of the scan rate in 1 M of Na_2SO_4. Nyquist plot (c) and complex capacitance (d) measured by electrochemical impedance spectroscopy at an AC potential of 10 mV and DC potential (vs. open circuit potential) in 1 M of Na_2SO_4: The inset of b shows the cyclic voltammograms of the black TiO_2 NTA as a function of the scan rate, and the inset of c shows an enlarged Nyquist plot of the high-frequency regions of the black TiO_2 NTA, respectively.

DOI: 10.1021/acsami.5b00123
ACS Appl. Mater. Interfaces 2015, 7, 7486–7491

of areal capacitance for black TiO_2 NTA and TiO_2 NTA were calculated by eq 4 with cyclic voltammograms.[41]

$$C = \frac{I_a - I_c}{2\nu \times A} \quad (4)$$

where C is the areal capacitance, ν is the potential scan rate (V/s), A_p is the apparent area (2.54 cm^2, d = 1.8 cm^2) of TiO_2 NTA, and $I_a - I_c$ is the anodic and cathodic current difference (A).

The surface characterization of black TiO_2 NTA was investigated with scanning electron microscopy (SEM, JSM-6700F, JEOL, Korea), high-resolution X-ray Diffraction (XRD, Bruker D8 DISCOVER, Germany), and X-ray photoelectron spectroscopy (XPS, SIGMA PROBE, ThermoVG, U.K).

3. RESULTS AND DISCUSSION

Figure 2a–c shows the surface characteristics of the black TiO_2 NTA examined by SEM images, XRD pattern, and XPS spectrum, respectively. As shown in Figure 2, there was no noticeable difference in the surface properties of the black TiO_2 NTA from the pristine TiO_2 NTA. For example, SEM image of the black TiO_2 NTA (Figure 2a) exhibited a highly ordered nanopore structure with an inner diameter of 80 nm, a thickness of 10 nm, and a tube length of 10 μm. The morphologies were similar to the pristine TiO_2 NTA (data not shown). The peak positions of black TiO_2 NTA in the XRD pattern (Figure 2b) was identically in agreement with that of the pristine TiO_2 NTA, indicating the anatase phase of the black TiO_2 NTA in the crystal structure. In addition, the overall XPS spectra in Figure 2c also exhibited no remarkable difference between the black TiO_2 NTA and the pristine TiO_2 NTA despite the slight negative shift of the Ti $2p_{3/2}$ and Ti $2p_{1/2}$ peaks (the inset of c) for the black TiO_2 NTA supporting the presence of Ti^{3+} states.[30]

Figure 3 shows the cyclic voltammograms of the black TiO_2 NTA compared with the pristine TiO_2 NTA. As can be seen in Figure 3, the black TiO_2 NTA exhibited a significantly different charging current density and oxygen evolution reaction (OER) from the pristine TiO_2 NTA. This vividly indicates the distinguished electrochemical properties of the black TiO_2 NTA with the pristine TiO_2 NTA. For example, the black TiO_2 NTA revealed a significantly higher charging current within 0.0–1.2 V of the potential range compared with the pristine TiO_2 NTA. In addition, oxygen was evidently generated on the black TiO_2 NTA under a potential of 1.2 V, whereas no OER was observed on the pristine TiO_2 NTA. These results suggest the potential of black TiO_2 NTA as a supercapacitor and an oxidant generating anode. Note that the red TiO_2 NTA did not reveal the high charging current density and OER (refer to Figure S3 in the Supporting Information).

Figure 4a–d shows the cyclic voltammograms within 0.0–0.8 V, and the areal capacitance obtained at the different scan rates (10, 50 100, 500, and 1000 mV/s), Nyquist plot, and complex capacitance of the black TiO_2 NTA exhibiting the capacitive properties compared with TiO_2 NTA, respectively. As shown in Figure 4a, the black TiO_2 NTA provided superior capacitive properties with nearly a rectangular shape for the cyclic voltammogram and a significantly higher value for the plateau current than that of the pristine TiO_2 NTA within 0.0–0.8 V of the potential range. It means that the black TiO_2 NTA exhibits an electrical double layer capacitor (EDLC)-like property.[42] The areal capacitance of the black TiO_2 NTA at a scan rate of 100 mV/s was ~15.6 mF/cm^2, and it has a significantly higher value than that of TiO_2 NTA (~0.1 mF/cm^2). Especially, this black TiO_2 NTA exhibited approximately 40% enhancement of areal capacitance in comparison with the annealed TiO_2 NTA

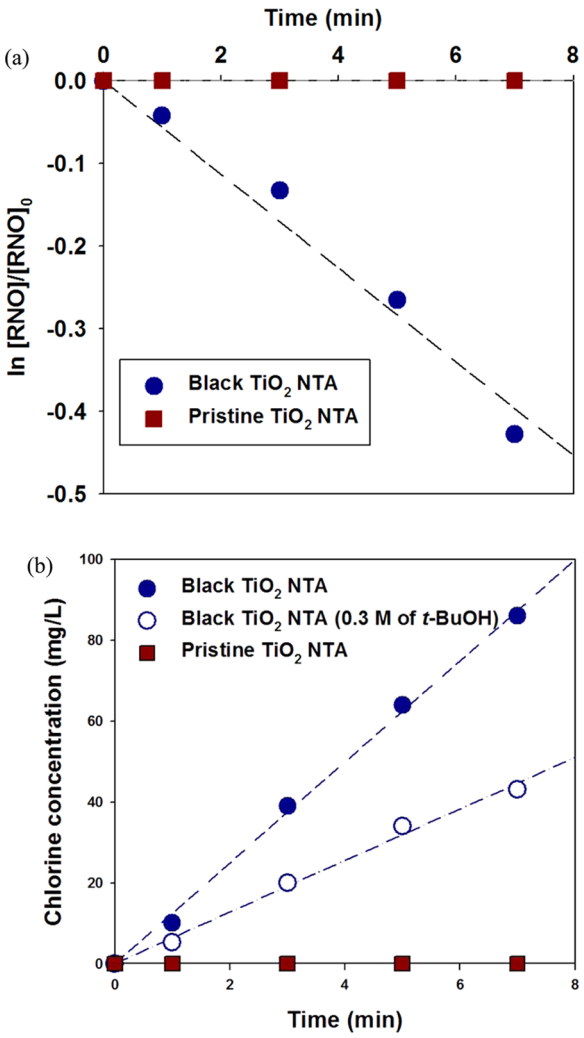

Figure 5. (a) Hydroxyl radical ($^{\bullet}OH$) generation ($[KH_2PO_4]_0$ = 0.1 M with NaOH (pH = 7.2), $[RNO]_0$ = 20 μM) and (b) evolution of chorine (Cl_2) on the black TiO_2 NTA and pristine TiO_2 NTA as an anode material ($[NaCl]_0$ = 0.1 M, $[t\text{-}BuOH]_0$ = 0.03 M) under constant current condition (i = 0.05 A/cm^2): The steady state production rate of the $^{\bullet}OH$s can be estimated by the slope of the semilog plot in panel a.

under N_2 without electrochemical self-doping (~11.6 mF/cm^2) (Figure S4a in Supporting Information). It indicates the electrochemical self-doping can provide the additional doping effect along with carbon doping (Figures S4b and S5 in Supporting Information). This carbon doping effect was attributed to the residual ethylene glycol on surface of TiO_2 NTA used as electrolyte in the anodization.[43]

Moreover, the magnitude of the areal capacitance of the black TiO_2 NTA at 1000 mV/s maintained more than 50% retention of that at 10 mV/s indicating a high power density of the black TiO_2 NTA (Figure 4b) and the capacitance retention reduces only ~4% for the 5000 cycles, suggesting the excellent capacitive behavior of the black TiO_2 NTA (Figure S6 in Supporting Information). These capacitive properties of the black TiO_2 NTA shown in Figure 4a and b can be strongly attributed to its enhanced electrical conductivity as a result of the cathodic polarization.[25,30,31] A notable difference in capacitive properties was also examined with the Nyquist plots and complex capacitance of the black TiO_2 NTA in Figure 4c and d. As shown in Figure 4c, the Nyquist plot of the black TiO_2 NTA

DOI: 10.1021/acsami.5b00123
ACS Appl. Mater. Interfaces 2015, 7, 7486–7491

revealed the vertical line started at 45° (inset of c) in the high and low frequency region indicating its good capacitive behavior.[44] On the other hand, in the plot of the pristine TiO_2 NTA, an approximately 45° impedance line (in the high frequency region in the inset of c) and depressed semicircular arc were observed, and this result is the typical shaped Nyquist plot of pristine TiO_2 NTA as proposed by the transmission line model.[30] This behavior of black TiO_2 NTA was also well supported by the larger magnitude of the double layer capacitance and a faster rate capability estimated, respectively, from the integrated area and position of the capacitive peak in the complex capacitance (Figure 4d) compared with that of the pristine TiO_2 NTA.[45]

Figure 5 shows the $^{\bullet}OH$ generation examined by RNO bleaching (a) and production of Cl_2 (b) on the black TiO_2 NTA compared to the pristine TiO_2 NTA.[39] The $^{\bullet}OH$ and Cl_2 are well-known as one of the strongest electro-generated oxidants.[46] The $^{\bullet}OH$ generation was investigated under chloride ion-free electrolyte conditions (1 M of KH_2PO_4 with NaOH), whereas evolution of Cl_2 was measured in 0.1 M NaCl. As shown in Figure 5, the $^{\bullet}OH$s (a) and Cl_2 (b) on the black TiO_2 NTA were evidently produced during electrolysis under a constant current condition (0.05 A/cm^2), whereas no production was observed on the pristine TiO_2 NTA. Especially, the excess *t*-BuOH as $^{\bullet}OH$ scavenger led to the partial inhibition of Cl_2 evolution on black TiO_2 NTA, suggesting that $^{\bullet}OH$ plays a critical role in Cl_2 generation.[29,39] These results indicates that the black TiO_2 NTA possesses a high electrocatalytic activity for $^{\bullet}OH$ and Cl_2 production.

Figure 6 shows the Mott–Schottky plot of the black TiO_2 NTA in comparison with that of the pristine TiO_2 NTA. The

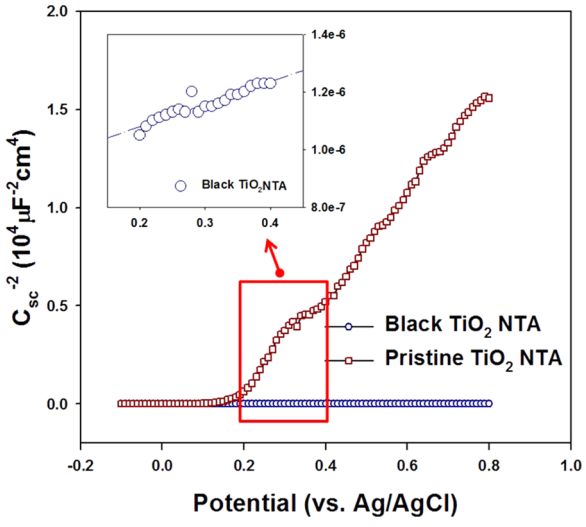

Figure 6. Mott–Schottky plot of black TiO_2 NTA and pristine TiO_2 NTA at an AC potential of 10 mV and frequency of 100 Hz ($[KH_2PO_4]_0$ = 1 M with NaOH (pH = 7.2)): The inset shows an enlarged plot of the black TiO_2 NTA showing the linearity of the Mott–Schottky slope in a potential range of 0.2–0.4 V.

black TiO_2 NTA had a much lower linear slope (the inset) than that of the pristine TiO_2 NTA indicating an enhanced charge carrier density on the black TiO_2 NTA. This increasing level of dopants is attributed to the cathodic polarization resulting from the trapped electrons (Ti^{3+} sites), or oxygen vacancies.[25,26] The high level of dopants can be an explanation for the superior capacitive and oxidant generating properties of the black TiO_2 NTA as proposed by previous studies.[30,31,33]

4. CONCLUSION

We report the novel capacitive and oxidant generating properties of black colored TiO_2 nanotube array (black TiO_2 NTA) fabricated by electrochemical self-doping of amorphous TiO_2 NTA and N_2 annealing. The fabricated black TiO_2 NTA exhibited stable and highly capacitive and electrocatalytic properties resulting in its good applications as a supercapacitor and an oxidant generating anode. These electrochemical features can be explained by the enhanced electronic properties of the black TiO_2 NTA-based on the increased level of dopants from electrochemical self-doping compared to the pristine TiO_2 NTA. This study suggests that black TiO_2 NTA can be applied as a supercapacitor and an oxidant generating anode.

■ ASSOCIATED CONTENT

Supporting Information

The XRD patterns, XPS spectra and additional experimental results were included in Figures S1–S6 to demonstrate the electrochemical properties of the Black TiO_2 NTA. This material is available free of charge via the Internet at http://pubs.acs.org.

■ AUTHOR INFORMATION

Corresponding Author

*E-mail: jeyong@snu.ac.kr. Phone: +82-2-880-8941. Fax: +82-2-876-8911.

Notes

The authors declare no competing financial interest.

■ ACKNOWLEDGMENTS

This research was supported by a grant (code 13IFIP-B065893-01) from Industrial Facilities & Infrastructure Research Program funded by Ministry of Land, Infrastructure, and Transport of Korean government.

■ REFERENCES

(1) Grimes, C. A.; Mor, G. K. *TiO_2 Nanotube Arrays: Synthesis, Properties, and Applications*; Springer: New York, 2009.
(2) Roy, P.; Berger, S.; Schmuki, P. TiO_2 Nanotubes: Synthesis and Applications. *Angew. Chem., Int. Ed.* **2011**, *50*, 2904–2939.
(3) Grimes, C. A. Synthesis and Application of Highly Ordered Arrays of TiO_2 Nanotubes. *J. Mater. Chem.* **2007**, *17*, 1451–1457.
(4) Tan, L. K.; Kumar, M. K.; An, W. W.; Gao, H. Transparent, Well-Aligned TiO_2 Nanotube Arrays with Controllable Dimensions on Glass Substrates for Photocatalytic Applications. *ACS Appl. Mater. Interfaces* **2010**, *2*, 498–503.
(5) Mor, G. K.; Shankar, K.; Paulose, M.; Varghese, O. K.; Grimes, C. A. Use of Highly-Ordered TiO_2 Nanotube Arrays in Dye-Sensitized Solar Cells. *Nano Lett.* **2006**, *6*, 215–218.
(6) Mor, G. K.; Varghese, O. K.; Paulose, M.; Shankar, K.; Grimes, C. A. A Review on Highly Ordered, Vertically Oriented TiO_2 Nanotube Arrays: Fabrication, Material Properties, and Solar Energy Applications. *Sol. Energy Mater. Sol. Cells* **2006**, *90*, 2011–2075.
(7) Huo, K.; Wang, H.; Zhang, X.; Cao, Y.; Chu, P. K. Heterostructured TiO_2 Nanoparticles/Nanotube Arrays: In Situ Formation from Amorphous TiO_2 Nanotube Arrays in Water and Enhanced Photocatalytic Activity. *ChemPlusChem* **2012**, *77*, 323–329.
(8) Xin, Y.; Jiang, J.; Huo, K.; Hu, T.; Chu, P. K. Bioactive $SrTiO_3$ Nanotube Arrays: Strontium Delivery Platform on Ti-Based Osteoporotic Bone Implants. *ACS Nano* **2009**, *3*, 3228–3234.

DOI: 10.1021/acsami.5b00123
ACS Appl. Mater. Interfaces 2015, 7, 7486–7491

(9) Hoffmann, M. R.; Martin, S. T.; Choi, W.; Bahnemann, D. W. Environmental Applications of Semiconductor Photocatalysis. *Chem. Rev.* **1995**, *95*, 69−96.
(10) Linsebigler, A. L.; Lu, G.; Yates, J. T., Jr Photocatalysis on TiO_2 Surfaces: Principles, Mechanisms, and Selected Results. *Chem. Rev.* **1995**, *95*, 735−758.
(11) Cho, M.; Cates, E. L.; Kim, J. H. Inactivation and Surface Interactions of MS-2 Bacteriophage in a TiO_2 Photoelectrocatalytic Reactor. *Water Res.* **2011**, *45*, 2104−2110.
(12) Albu, S. P.; Ghicov, A.; Macak, J. M.; Hahn, R.; Schmuki, P. Self-organized, Free-Standing TiO_2 Nanotube Membrane for Flow-through Photocatalytic Applications. *Nano Lett.* **2007**, *7*, 1286−1289.
(13) Sun, W. T.; Yu, Y.; Pan, H. Y.; Gao, X.-F.; Chen, Q.; Peng, L. M. CdS Quantum Dots Sensitized TiO_2 Nanotube-Array Photoelectrodes. *J. Am. Chem. Soc.* **2008**, *130*, 1124−1125.
(14) Zhang, X.; Huo, K.; Hu, L.; Wu, Z.; Chu, P. K. Synthesis and Photocatalytic Activity of Highly Ordered TiO_2 and $SrTiO_3/TiO_2$ Nanotube Arrays on Ti Substrates. *J. Am. Ceram. Soc.* **2010**, *93*, 2771−2778.
(15) Wang, G.; Wang, H.; Ling, Y.; Tang, Y.; Yang, X.; Fitzmorris, R. C.; Wang, C.; Zhang, J. Z.; Li, Y. Hydrogen-treated TiO_2 Nanowire Arrays for Photoelectrochemical Water Splitting. *Nano Lett.* **2011**, *11*, 3026−3033.
(16) Salari, M.; Aboutalebi, S. H.; Konstantinov, K.; Liu, H. K. A Highly Ordered Titania Nanotube Array as a Supercapacitor Electrode. *Phys. Chem. Chem. Phys.* **2011**, *13*, 5038−5041.
(17) Yang, Y.; Kim, D.; Yang, M.; Schmuki, P. Vertically Aligned Mixed V_2O_5−TiO_2 Nanotube Arrays for Supercapacitor Applications. *Chem. Commun.* **2011**, *47*, 7746−7748.
(18) Ambade, R. B.; Ambade, S. B.; Shrestha, N. K.; Nah, Y. C.; Han, S. H.; Lee, W.; Lee, S. H. Polythiophene Infiltrated TiO_2 Nanotubes as High-Performance Supercapacitor Electrodes. *Chem. Commun.* **2013**, *49*, 2308−2310.
(19) Xu, J.; Wu, H.; Lu, L.; Leung, S. F.; Chen, D.; Chen, X.; Fan, Z.; Shen, G.; Li, D. Integrated Photo-Supercapacitor Based on Bi-polar TiO_2 Nanotube Arrays with Selective One-Side Plasma-Assisted Hydrogenation. *Adv. Funct. Mater.* **2014**, *24*, 1840−1846.
(20) Zhao, R.; Biesheuvel, P.; Van der Wal, A. Energy Consumption and Constant Current Operation in Membrane Capacitive Deionization. *Energy Environ. Sci.* **2012**, *5*, 9520−9527.
(21) Macak, J.; Tsuchiya, H.; Ghicov, A.; Yasuda, K.; Hahn, R.; Bauer, S.; Schmuki, P. TiO_2 Nanotubes: Self-Organized Electrochemical Formation, Properties and Applications. *Curr. Opin. Solid State Mater. Sci.* **2007**, *11*, 3−18.
(22) Chen, X.; Liu, L.; Peter, Y. Y.; Mao, S. S. Increasing Solar Absorption for Photocatalysis with Black Hydrogenated Titanium Dioxide Nanocrystals. *Science* **2011**, *331*, 746−750.
(23) Lu, X.; Wang, G.; Zhai, T.; Yu, M.; Gan, J.; Tong, Y.; Li, Y. Hydrogenated TiO_2 Nanotube Arrays for Supercapacitors. *Nano Lett.* **2012**, *12*, 1690−1696.
(24) Kesselman, J. M.; Weres, O.; Lewis, N. S.; Hoffmann, M. R. Electrochemical Production of Hydroxyl Radical at Polycrystalline Nb-Doped TiO_2 Electrodes and Estimation of the Partitioning between Hydroxyl Radical and Direct Hole Oxidation Pathways. *J. Phys. Chem.B* **1997**, *101*, 2637−2643.
(25) Fabregat-Santiago, F.; Barea, E. M.; Bisquert, J.; Mor, G. K.; Shankar, K.; Grimes, C. A. High Carrier Density and Capacitance in TiO_2 Nanotube Arrays Induced by Electrochemical Doping. *J. Am. Chem. Soc.* **2008**, *130*, 11312−11316.
(26) Macak, J. M.; Gong, B. G.; Hueppe, M.; Schmuki, P. Filling of TiO_2 Nanotubes by Self-Doping and Electrodeposition. *Adv. Mater.* **2007**, *19*, 3027−3031.
(27) Tokudome, H.; Miyauchi, M. Electrochromism of Titanate-Based Nanotubes. *Angew. Chem., Int. Ed.* **2005**, *44*, 1974−1977.
(28) Ghicov, A.; Tsuchiya, H.; Hahn, R.; Macak, J. M.; Muñoz, A. G.; Schmuki, P. TiO_2 Nanotubes: H^+ Insertion and Strong Electrochromic Effects. *Electrochem. Commun.* **2006**, *8*, 528−532.
(29) Kim, C.; Kim, S.; Choi, J.; Lee, J.; Kang, J. S.; Sung, Y. E.; Lee, J.; Choi, W.; Yoon, J. Blue TiO_2 Nanotube Array as an Oxidant Generating Novel Anode Material Fabricated by Simple Cathodic Polarization. *Electrochim. Acta* **2014**, *141*, 113−119.
(30) Zhou, H.; Zhang, Y. Electrochemically Self-Doped TiO_2 Nanotube Arrays for Supercapacitors. *J. Phys. Chem. C* **2014**, *118*, 5626−5636.
(31) Wu, H.; Li, D.; Zhu, X.; Yang, C.; Liu, D.; Chen, X.; Song, Y.; Lu, L. High-Performance and Renewable Supercapacitors Based on TiO_2 Nanotube Array Electrodes Treated by an Electrochemical Doping Approach. *Electrochim. Acta* **2014**, *116*, 129−136.
(32) Li, H.; Chen, Z.; Tsang, C. K.; Li, Z.; Ran, X.; Lee, C.; Nie, B.; Zheng, L.; Hung, T.; Lu, J. Electrochemical Doping of Anatase TiO_2 in Organic Electrolytes for High-performance Supercapacitors and Photocatalysts. *J. Mater. Chem. A* **2014**, *2*, 229−236.
(33) Zheng, Q.; Lee, H. J.; Lee, J.; Choi, W.; Park, N. B.; Lee, C. Electrochromic Titania Nanotube Arrays for the Enhanced Photocatalytic Degradation of Phenol and Pharmaceutical Compounds. *Chem. Eng. J.* **2014**, *249*, 285−292.
(34) Fang, H. T.; Liu, M.; Wang, D. W.; Sun, T.; Guan, D. S.; Li, F.; Zhou, J.; Sham, T. K.; Cheng, H. M. Comparison of the Rate Capability of Nanostructured Amorphous and Anatase TiO_2 for Lithium Insertion Using Anodic TiO_2 Nanotube Arrays. *Nanotechnology* **2009**, *20*, 225701.
(35) Xiong, H.; Slater, M. D.; Balasubramanian, M.; Johnson, C. S.; Rajh, T. Amorphous TiO_2 Nanotube Anode for Rechargeable Sodium Ion Batteries. *J. Phys. Chem. Lett.* **2011**, *2*, 2560−2565.
(36) Kim, C.; Park, H. J.; Cha, S.; Yoon, J. Facile Detection of Photogenerated Reactive Oxygen Species in TiO_2 Nanoparticles Suspension Using Colorimetric Probe-Assisted Spectrometric Method. *Chemosphere* **2013**, *93*, 2011−2015.
(37) Muff, J.; Bennedsen, L.; Søgaard, E. G. Study of Electrochemical Bleaching of *p*-Nitrosodimethylaniline and Its Role as Hydroxyl Radical Probe Compound. *J. Appl. Electrochem.* **2011**, *42*, 599−607.
(38) Simonsen, M. E.; Muff, J.; Bennedsen, L. R.; Kowalski, K. P.; Søgaard, E. G. Photocatalytic Bleaching of *p*-Nitrosodimethylaniline and a Comparison to the Performance of Other AOP Technologies. *J. Photochem. Photobiol., A* **2010**, *216*, 244−249.
(39) Jeong, J.; Kim, C.; Yoon, J. The Effect of Electrode Material on the Generation of Oxidants and Microbial Inactivation in the Electrochemical Disinfection Processes. *Water Res.* **2009**, *43*, 895−901.
(40) Bard, A. J.; Faulkner, L. R. *Electrochemical Methods: Fundamentals and Applications*; Wiley: New York, 1980.
(41) Kim, C.; Lee, J.; Kim, S.; Yoon, J. TiO_2 Sol−Gel Spray Method for Carbon Electrode Fabrication to Enhance Desalination Efficiency of Capacitive Deionization. *Desalination* **2014**, *342*, 70−74.
(42) Frackowiak, E.; Beguin, F. Carbon Materials for the Electrochemical Storage of Energy in Capacitors. *Carbon* **2001**, *39*, 937−950.
(43) Hu, L.; Huo, K.; Chen, R.; Gao, B.; Fu, J.; Chu, P. K. Recyclable and High-Sensitivity Electrochemical Biosensing Platform Composed of Carbon-Doped TiO_2 Nanotube Arrays. *Anal. Chem.* **2011**, *83*, 8138−8144.
(44) Fabregat-Santiago, F.; Garcia-Belmonte, G.; Bisquert, J.; Zaban, A.; Salvador, P. Decoupling of Transport, Charge Storage, and Interfacial Charge Transfer in the Nanocrystalline TiO_2/electrolyte System by Impedance Methods. *J. Phys. Chem. B* **2002**, *106*, 334−339.
(45) Jang, J. H.; Yoon, S.; Bok, H. K.; Jung, Y.-H.; Oh, S. M. Complex Capacitance Analysis on Leakage Current Appearing in Electric Double-Layer Capacitor Carbon Electrode. *J. Electrochem. Soc.* **2005**, *152*, A1418−A1422.
(46) Martínez-Huitle, C. A.; Brillas, E. Electrochemical Alternatives for Drinking Water Disinfection. *Angew. Chem., Int. Ed.* **2008**, *47*, 1998−2005.

DOI: 10.1021/acsami.5b00123
ACS Appl. Mater. Interfaces 2015, 7, 7486−7491